Int J Adv Manuf Technol (2017) 92:3197–3206
DOI 10.1007/s00170-017-0390-2

ORIGINAL ARTICLE

Error analysis and improved calibration algorithm for LED chip localization system based on visual feedback

Ziyue Wang[1] · **Shihua Gong**[1] · **Delong Li**[1] · **Huaiqing Lu**[1]

Received: 5 December 2016 / Accepted: 3 April 2017 / Published online: 20 April 2017

Abstract Positioning accuracy of chip directly impacts on the quality and efficiency of LED chip production. The purpose of this paper is to improve the chip positioning accuracy by improving the camera calibration algorithm of LED chip visual positioning system. Firstly, by making the error analysis for the visual positioning system, the systematic errors of each parts of the system are obtained, and the relationship between chip positioning error and chip position distribution in image is found. Then, according to the result of error analysis and the characteristics of the chip positioning process, an improved calibration algorithm is proposed to improve the chip positioning accuracy. This improved algorithm solves the calibration parameters in two steps, which highlights the main cause of errors in calibration process and meets the requirements of chip positioning. Finally, the experiment results show that the proposed algorithm can improve the chip positioning accuracy obviously, and has good stability and robustness.

Keywords LED chip · Visual positioning · Error analysis · Calibration algorithm

1 Introduction

As the fourth generation of green lighting source, LED has been applied to many industries and fields, such as electronic industry, automotive lights, display, lighting, traffic lights, and so on. In the LED manufacturing process, detection and sorting of LED chips directly affect the LED production quality and efficiency, and therefore high-speed and high-precision positioning control of LED chips has been research priorities of the field [1]. In the development and improvement of LED manufacturing equipment, machine vision has been widely used in identifying and positioning of LED chips. To improve accuracy and efficiency of chip positioning, many scholars have been committed to researching robust control algorithms, accurate image recognition, real-time visual feedback, and other issues [2]. However, as the first step of the visual positioning, the camera calibration technology research in LED manufacturing equipment has been little investigated and is also worthy of attention.

As the development of machine vision, camera calibration theory and technology has also been developed, and many scholars in different areas have proposed corresponding calibration algorithm [3]. So far, there have been three kinds of camera calibration technology: the traditional calibration, based on active vision calibration and self-calibration. The traditional calibration method, which requires a calibration object of known shape and size, includes nonlinear calibration method proposed by Faig [4], Direct Linear Transformation method [5], two-step method proposed by Tsai [6], and iterative method (improved two-step method) proposed by Weng et al. [7]. In spite of high precision, this method is not suitable for high-speed and high-efficiency LED production because of the complex calibration process and excessive dependence on calibration object. To solve this problem, Faugeras et al. [8] proposed the self-calibration method, which were adept in the simple calibration process without calibration object. Developing since its inception, there have been the QR decomposition method [9], the absolute quadric surface method [10, 11], and the modular constraint method [12, 13]. In

✉ Shihua Gong
gongshihua1@mail.hust.edu.cn

[1] State Key Lab of Digital Manufacturing and Equipment Technology, Huazhong University of Science and Technology, Wuhan 430074, China

Galetto et al. [14], the network self-calibration was utilized for indoor coordinate measuring system for large-scale metrology applications. Li has solved the self-calibration problem by using and particle swarm optimization algorithm (GA-PSO) [15], while Akkad used Levenberg-Marquardt algorithm and improved genetic algorithm [16, 17]. Bellandi et al. [18] integrated calibration procedures into 2D and 3D vision of Roboscan, which performed well in a number of pick-and-place operations. Muruganantham et al. [19] was devoted to studying the optimal settings for vision camera calibration and improved accuracy and repeatability of calibration. Nevertheless, the self-calibration technology had not been widely applied to chip visual positioning on account of its low accuracy and high demand for high-performance vision and motion control system. Consequently, a based on active vision calibration method, which had a simpler calibration process than the traditional calibration method, was proposed based on self-calibration technology, and had a higher accuracy compared with the self-calibration technology. The based on active vision calibration method included the based on camera rotation calibration method [20], the based on camera orthogonal translation calibration method [21], and the based on camera plane orthogonal motion calibration method [22]. Shih and Ruo used auto-calibration method to improve the accuracy of SMT machine [23], which did not need expensive calibration instruments and had little calibration time. Zhan et al. [24] applied hand–eye calibration to positioning for a robot drilling system and analyzed the main factors that affect the positioning error.

However, besides high efficiency and high precision, the chip localization system has its own characteristics, such as different types and sizes of chips, frequent replacement of wafer and deformation of wafer membrane, and the need to adjust magnification of lens, focal length, and relative location of *X*–*Y* table and vision system, which may somehow change calibration parameters, especially in the high magnification. Therefore, it is necessary to propose a new calibration algorithm to improve positioning accuracy and efficiency of LED chip. This paper proposed the improved calibration algorithm applied to LED chip visual localization system. The second part mainly introduces the hardware and software of the visual localization system. In the third part, by making the error analysis for the visual localization system, the systematic errors of each part of the system are obtained, and the relationship between chip positioning error and chip position distribution is found. In the fourth part, according to the result of error analysis and the characteristics of the chip localization system, an improved calibration algorithm is proposed. The validity and robustness of the algorithm are verified by experiments in the fifth part.

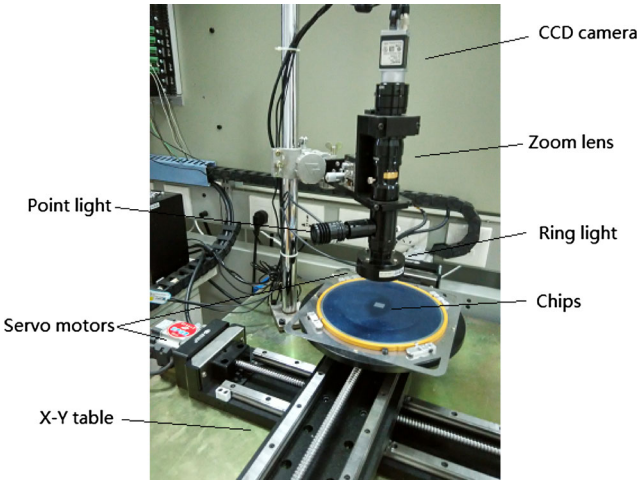

Fig. 1 Visual localization system

2 LED chip localization system based on visual feedback

2.1 Hardware and structure of the system

The visual localization system described in this paper is composed of motion control system and vision system. The motion control system consists of a ball screw-driven *X*–*Y* table, a motion controller, and two AC servo motors. *X*–*Y* table has a maximum speed of 500 mm/s, a maximum stroke of 300 mm × 300 mm, and repeatability of 5 μm to meet the requirements of high-speed and high-precision motion control. To ensure fast response and exceeding stability, a dual-axes motion control card, which has a servo cycle of 442 μs, and two AC servo motors with servo drivers are selected. Owing to the tiny size of chip, dense arrangement, and dispersion of ambient light, high-performance CCD camera, continuous zoom coaxial fine-tuning lens, and controllable point light and ring light are used to improve the position identification accuracy of LED chip. The visual localization system is shown in Fig. 1. In order to achieve the high-speed and high-precision requirements for chip positioning, a closed-loop motion control system based on visual feedback and coarse-fine two-step positioning strategy are adopted in this paper, as shown in Fig. 2. Chip's rapid movement and coarse positioning are completed through the motor encoder feedback, and the closed-loop structure based on visual feedback performs compensation of errors and accurate positioning of chip.

2.2 Image processing

As the core of the visual system, image processing directly affects the chip position identification precision and efficiency. This research proposed the chip positioning algorithm based on sub-pixel edge detection, which did not need to train the template artificially and improved the accuracy of edge

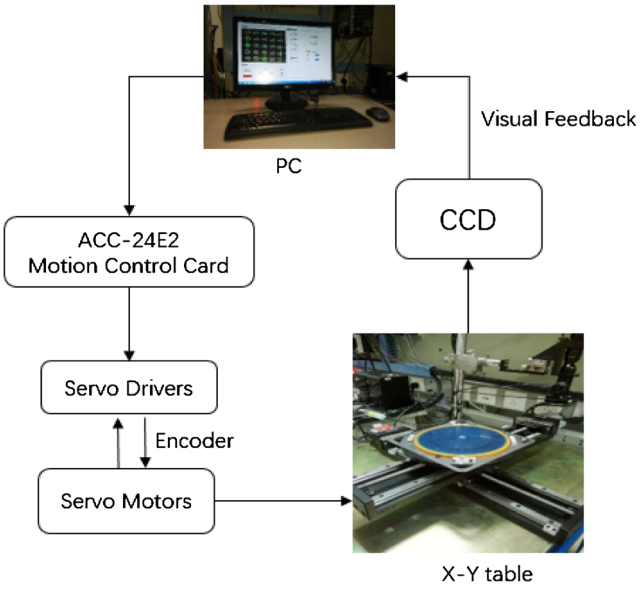

Fig. 2 System structure diagram

extraction. The image processing flow diagram is shown in Fig. 3. Firstly, the image captured through the CCD camera must be preprocessed to reduce the impact of uneven background light. Secondly, the image preprocessed is segmented by Otsu algorithm to obtain the approximate area of chips and optimized by Blob algorithm to remove the defect spot and extract the chip area. Thirdly, the outer contour region of the chip is obtained through the minimum circumscribed rectangle method, and then the chip sub-pixel edge contour is extracted by canny algorithm. Fourthly, as the sub-pixel edge

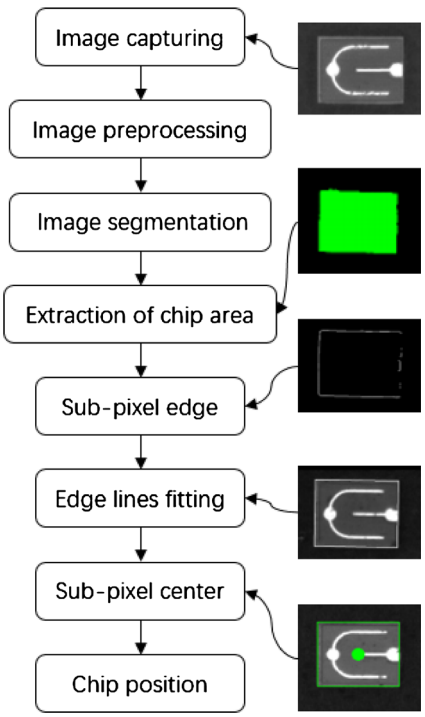

Fig. 3 Image processing flow diagram

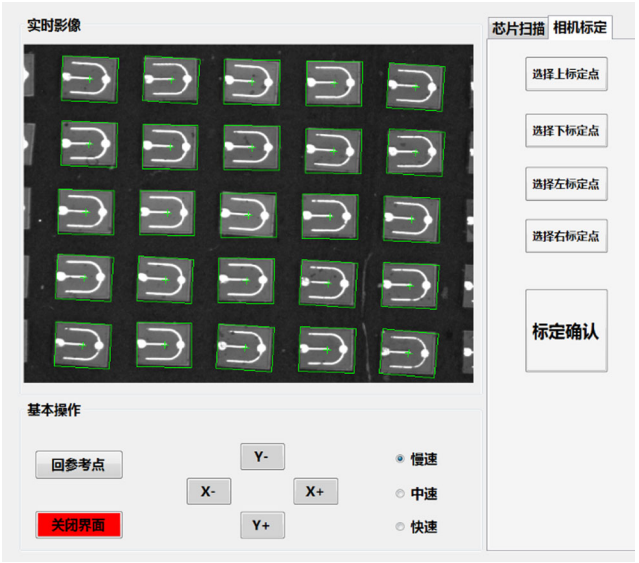

Fig. 4 User interface

extracted by canny algorithm is imperfect, the linear fitting is used to fitting the sub-pixel edge contour. Finally, the position geometrical information of chip can be obtained through rectangular sub-pixel edge contour. Realization of image processing algorithm, real-time monitoring of chip positioning, and some basic operations are realized by the user interface based on Visual Studio software on PC, as shown in Fig. 4.

3 Error analysis of system

3.1 Error of image processing

To detect the identification accuracy of the image processing algorithm described in Section 2.2, we designed an experiment here. In the experiment, capturing ten images while *X*–*Y* table did not move, we could obtain the position geometrical information of chips in each image through the image processing algorithm. The repeatability of the chip position detection depended on the image processing algorithm, the ambient light disturbance, and noise. We selected one of the chips and recorded its pixel coordinates in these ten images, as shown in Fig. 5. The result showed that the repeatability of the chip position detection was 0.5 pixel. By converting the pixel coordinates to world coordinates, the systematic error of image processing was ±3 μm.

3.2 Error of motion control system

As described in Section 2.1, we adopt coarse-fine two-step positioning strategy, and Fig. 6 shows the control system block diagram. Therefore, the error of motion control system comes from two aspects.

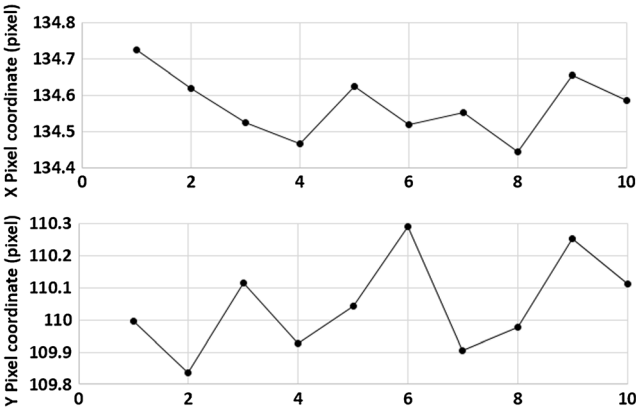

Fig. 5 Image processing repeatability test

The first part of error source is caused in the process of chip's rapid movement and coarse positioning. The measurement results of frequency characteristic of *X*–*Y* table are shown in Figs. 7 and 8, and we found that they had a wide bandwidth and good stability to ensure the high-speed and high-precision motion control of *X*–*Y* table. The positioning errors of *X*-axis and *Y*-axis have been measured with a laser displacement sensor, and the results showed that the positioning accuracy is ±2 μm.

The other part of the error source comes from accurate positioning with closed-loop system based on visual feedback. This error is affected by some factors, such as deformation of wafer membrane, systematic error of controller, environment disturbance, noise, etc. These factors are nonlinear and are affected by multiple parameters, so that their solution is complex and inaccurate. Therefore, the visual feedback method is used to compensate for these errors in this research. To test the positioning error of visual feedback, 25 chips in an image were positioned with a common calibration algorithm. Figures 9 and 10 respectively showed the positioning errors before compensation and after compensation. The results showed that positioning error had been significantly reduced, but was still great and must be further reduced.

3.3 Camera calibration

For a system that consists of motion control and machine vision, the camera calibration directly affects the accuracy of

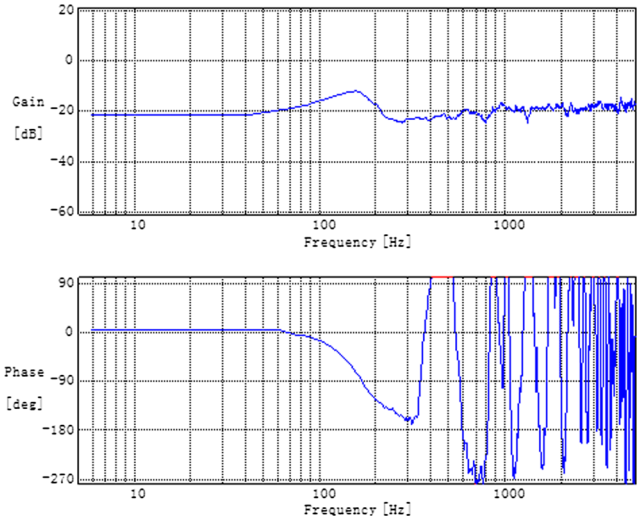

Fig. 7 *X*-axis frequency characteristic

the overall system. As the visual localization system described in this paper is mainly used in two-dimensional positioning of chip, camera external parameters become the focus of this research, while the influence from the camera internal parameters is small. Camera external parameters are mainly affected by manufacturing and installation errors of camera, lens, and other visual devices. As shown in Fig. 11, the angle denoted by α between the camera image plane (red) and the chip plane (black) in the Z direction, and the angles denoted by β and γ respectively in the Y and X direction, will be analyzed and solved in this research.

Firstly, the error caused by the angle α between the camera image plane and the chip plane in the Z direction is analyzed. As shown in Fig. 12, when the chip moves from the point q to q', the movement distance in image coordinate of the chip is (p_x, p_y), while the theoretical movement distance of chip should be (w_x, w_y). Eq. (1) is obtained after simple geometric inference, where s is the pixel-distance conversion coefficient and (u, v) is the pixel coordinate. The positioning errors caused by α are calculated in Eq. (2). As shown in Eq. (2), when $\alpha > 0$, the errors of chips in the upper left and lower right sides (p_x and p_y symbols are opposite in sign) of the image are relatively larger, while the errors of chips in the lower left and upper right sides (p_x and p_y symbols are same in sign) of the image are relatively smaller, and the farther away from the

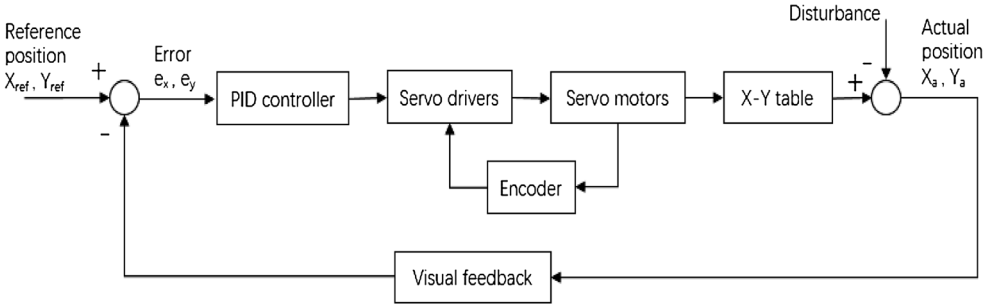

Fig. 6 Control system block diagram

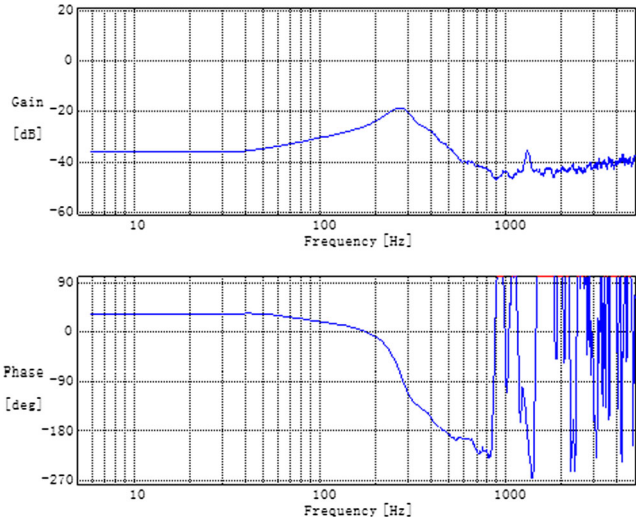

Fig. 8 *Y*-axis frequency characteristic

localization point the chips, the greater the errors. Since α is generally small, the errors in X direction e_x of the chips in the different rows have a larger difference relatively and increase gradually from top to bottom of the image, while the errors in Y direction e_y in the different columns have also larger difference relatively and decrease gradually from left to right of the image. The case when α <0 is similar to the case when α >0, and the greater the absolute value of α, the more obvious these phenomena. Figure 13 shows the image of chips taken by CCD camera, and the localization point is the center of the image. Positioning these chips, the positioning errors are recorded in Table 1, and obviously the relationship between the position errors and the chip position distribution was consistent with the analysis above.

$$\begin{aligned} w_x &= p_x\cos\alpha - p_y\sin\alpha = s\cdot u\cdot\cos\alpha - s\cdot v\cdot\sin\alpha \\ w_y &= p_y\cos\alpha + p_x\sin\alpha = s\cdot v\cdot\cos\alpha + s\cdot u\cdot\sin\alpha \end{aligned} \tag{1}$$

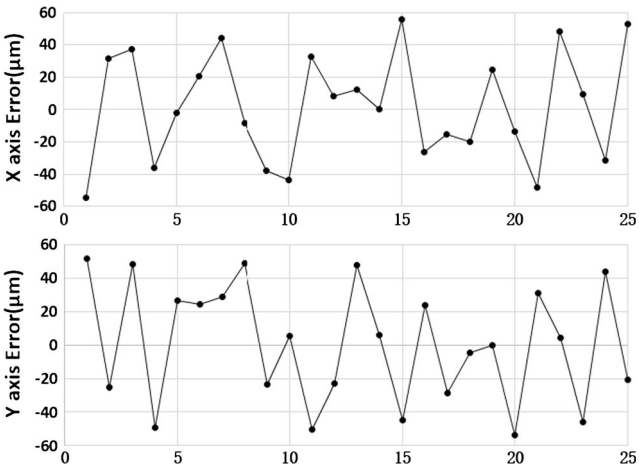

Fig. 9 Before visual compensation

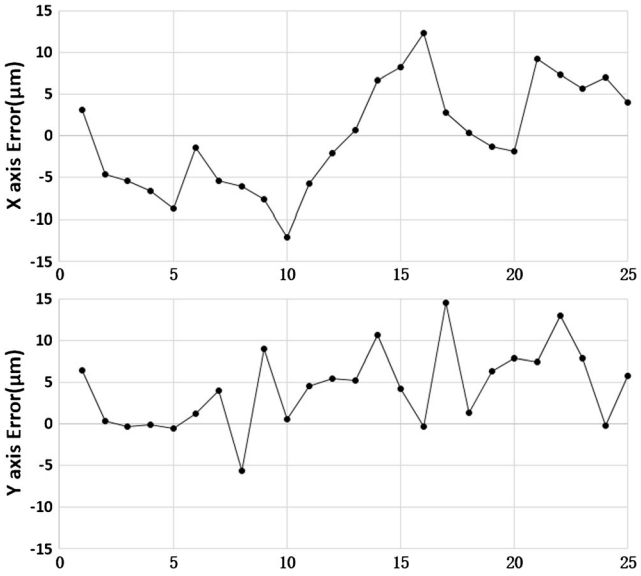

Fig. 10 After visual compensation

$$\begin{aligned} e_x &= p_x - w_x = p_x\cdot(1-\cos\alpha) + p_y\sin\alpha \\ e_y &= p_y - w_y = p_y\cdot(1-\cos\alpha) - p_x\sin\alpha \end{aligned} \tag{2}$$

Then, the errors caused by the angle β between the camera image plane and the chip plane in the Y direction are analyzed. As shown in Fig. 14, when the chip moves from the point q_1 or q_2 to the localization point q_0, the movement distance in image coordinate and the theoretical movement distance of the chip are respectively p_x and w_x, and their relationship is given by Eq. (3). Eq. (4) shows the positioning error caused by β. As described in Eq. (3) and Eq. (4), regardless of sign of β, the position errors of chips in the left side ($p_x > 0$) of the image are negative, while the errors of chips in the right side ($p_x < 0$) of the image are positive, and the positioning errors increase linearly with the distance from the localization point. The case of the angle γ between the camera image plane and the chip plane in the X direction is similar to β. As described in Eq. (5)

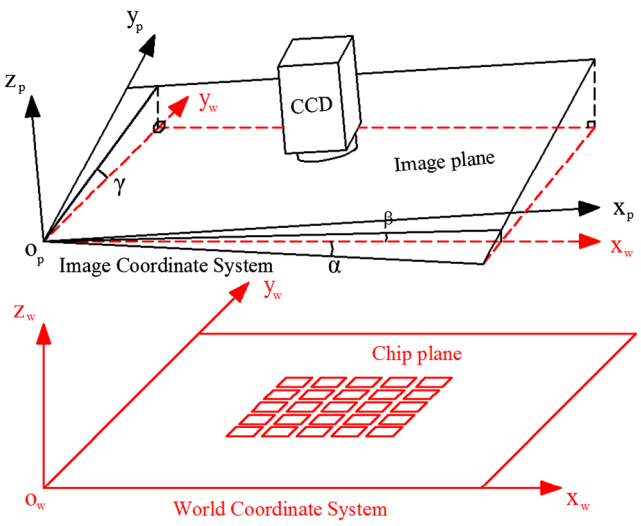

Fig. 11 Vision system diagram

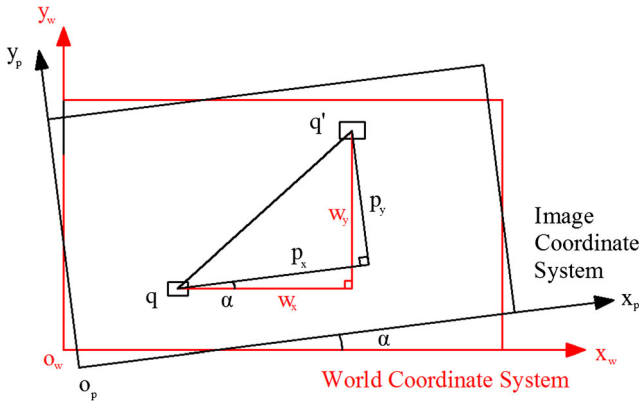

Fig. 12 *X–Y* plane diagram

and Eq. (6), regardless of sign of γ, the positioning errors of chips in the bottom side ($p_y > 0$) of the image are negative, while the errors of chips in the top side ($p_y < 0$) of the image are positive, and the positioning errors increase linearly with the distance from the localization point. Similarly, the greater the absolute value of β and γ, the more obvious these phenomena.

$$w_x = p_x \Big/ \cos\beta = s{\cdot}u \Big/ \cos\beta \tag{3}$$

$$e_x = p_x - w_x = p_x{\cdot}\left(1 - 1 \Big/ \cos\beta\right) \tag{4}$$

$$w_y = p_y \Big/ \cos\gamma = s{\cdot}u \Big/ \cos\gamma \tag{5}$$

$$e_y = p_y - w_y = p_y{\cdot}\left(1 - 1 \Big/ \cos\gamma\right) \tag{6}$$

In conclusion, the positioning errors of chips are obviously closely related to the position distribution of chips in image. We thence can solve α, β, and γ through the relationship between the chip positioning errors and the position distribution of chips in image to improve the positioning accuracy of chips.

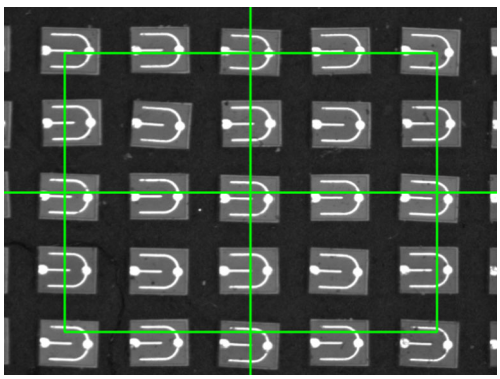

Fig. 13 Image of chips

4 Calibration algorithm

4.1 Common calibration algorithm

Now, the calibration method used in most of the chip visual positioning systems is to solve the transformation matrix in Eq. (7), namely the rotation matrix R and translation matrix t. The calibration parameters R and t obtained by this method almost contain all of the required calibration information, and this method is therefore widely used. However, it requires multiple sets of measurements of $[x_p, y_p, z_p]^T$ and $[x_w, y_w, z_w]^T$ to solve the transformation matrix R and t, which increases computational complexity and reduces efficiency. In particular, because of the two-dimensional motion of chip, z_p and z_w are difficult to measure with only one CCD camera, and solving the calibration parameters in two-dimensional plane (ignoring z_p and z_w) may impact on the positioning accuracy. Moreover, chip visual positioning system has its own characteristics. After frequent replacement of wafer, in order to get clear and satisfactory image, we should adjust the magnification of lens, focal length, and relative location of *X–Y* table and vision system to different types and sizes of chips. During the adjusting process, a tiny position change of the CCD camera fixed on zoom lens on horizontal plane may make the angle α vary and become relatively greater in high magnification, while the absolute value of angles β and γ are relatively smaller and remain almost constant because of the better verticality and parallelism of the installation of the vision system. However, the common calibration algorithm has no regard for these phenomena, which brings greater errors. As shown in Figs. 9 and 10, the positioning errors with common calibration algorithm were about ±15 μm, but in the high-quality and efficient manufacturing of chips, the positioning errors were generally less than 10 μm.

$$\begin{bmatrix} x_p \\ y_p \\ z_p \\ 1 \end{bmatrix} = \begin{bmatrix} \mathrm{R} & \mathrm{t} \\ 0 & 1 \end{bmatrix} \cdot \begin{bmatrix} x_w \\ y_w \\ z_w \\ 1 \end{bmatrix} \tag{7}$$

4.2 Improved calibration algorithm

According to the characteristics of chip visual positioning, an improved calibration algorithm is proposed in this research. The improved algorithm separates the calibration process into two steps: solving α first and then solving β and γ, instead of solving the transformation matrix at a time in common calibration algorithm, and improving calibration efficiency and chip positioning accuracy.

As described in Section 3.3, we solve α, β, and γ through the relationship between chip positioning errors and the position distribution of chips in image. Firstly, the method of

Table 1 The position distribution and the positioning errors

Positioning Error (μm)		Column				
		1	2	3	4	5
Row	1	(−56.03, 49.71)	(−49.91, 25.28)	(−45.76, 0.96)	(−40.49, −29.40)	(−37.50, −55.55)
	2	(−29.99, 47.86)	(−32.08, 25.55)	(−23.03, −7.15)	(−16.87, −36.83)	(−15.47, −58.50)
	3	(−5.94, 44.30)	(−2.93, 25.50)	(−1.36, 1.02)	(5.46, −28.91)	(7.98, −54.49)
	4	(13.87, 50.75)	(14.98, 24.06)	(22.17, −3.82)	(28.30, −31.14)	(30.87, −55.28)
	5	(36.63, 43.91)	(42.08, 31.71)	(45.81, 4.08)	(51.59, −24.87)	(53.39, −50.64)

solving α is introduced. Eq. (8) is obtained by eliminating the sinα term from the two equations in Eq. (2):

$$p_x \cdot e_x + p_y \cdot e_y = \left(p_x^2 + p_y^2\right) \cdot (1 - \cos\beta) \tag{8}$$

By substituting $Y = p_x \cdot e_x + p_y \cdot e_y$ and $X = p_x^2 + p_y^2$ into Eq. (8):

$$Y = (1 - \cos\beta) \cdot X \tag{9}$$

Obtaining the experimental data (X_i, Y_i) (i = 1,2,…N), we can solve the slope $k_\alpha = 1 - \cos\alpha$ with linear fitting. According to least square method:

$$\frac{\partial \sum (Y_i - k_\alpha \cdot X_i)^2}{\partial k_\alpha} = 0 \qquad (i = 1, 2 \ldots N) \tag{10}$$

Solving Eq. (10):

$$k_\alpha = \frac{\sum X_i Y_i}{\sum X_i^2} \qquad (i = 1, 2 \ldots N) \tag{11}$$

where $Y_i = p_{xi} \cdot e_{xi} + p_{yi} \cdot e_{yi}$, $X_i = p_{xi}^2 + p_{yi}^2$, and N is the number of chips selected in an image. Generally, we select five chips scattered in image (N = 5). Solving k_α, we can obtain $\cos\alpha = 1 - k_\alpha$.

Then, we solve the angles β and γ. As shown in Eq. (4), similarly, obtaining the experimental data (p_{xi}, e_{xi}) (i = 1,2,…

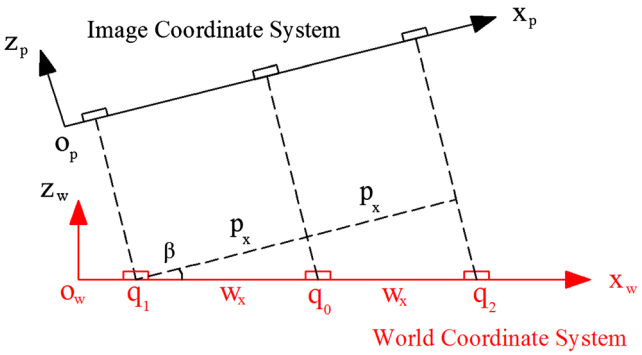

Fig. 14 *X–Z* plane diagram

N), we can solve the slope $k_\beta = 1 - 1/\cos\beta$ with linear fitting. According to least square method:

$$\frac{\partial \sum \left(e_{xi} - k_\beta \cdot p_{xi}\right)^2}{\partial k_\beta} = 0 \qquad (i = 1, 2 \ldots N) \tag{12}$$

Solving Eq. (12):

$$k_\beta = \frac{\sum p_{xi} e_{xi}}{\sum p_{xi}^2} \qquad (i = 1, 2 \ldots N) \tag{13}$$

where N is the number of chips selected in image. Similarly, we select five chips scattered in image(N = 5). Solving k_β, we can obtain $\cos\beta = 1/(1 - k_\beta)$. The solution of the angle γ is the same as β, and we can obtain $\cos\gamma = 1/(1 - k_\gamma)$.

Where

$$k_\gamma = \frac{\sum p_{yi} e_{yi}}{\sum p_{yi}^2} \qquad (i = 1, 2, 3, 4, 5) \tag{14}$$

As analyzed in Section 4.1, the angle α may vary and is generally relatively greater, while the angles β and γ are relatively smaller and remain almost constant, so the angle α should be solved and compensated first in improved calibration algorithm. Improving calibration algorithm with α, we position the chips in one image and get the positioning errors of the chips, which should be compared with the systematic error. If the positioning errors are greater than the systematic error, the errors caused by the angles β and γ cannot be ignored and we should solve and compensate β and γ. On the contrary, if the positioning errors are smaller than the systematic error, we can consider the angles β and γ are extremely small and ignored. The improved calibration algorithm solves the calibration parameters in two steps and decides the solution of α, β, and γ according to the relationship between positioning errors and systematic error, which effectively improves calibration efficiency and chip positioning accuracy. As analyzed in Sections 3.1 and 3.2, we can consider the systematic error of the localization system based on visual feedback described in this paper is about 6 μm. The improved calibration algorithm flow diagram is shown in Fig. 15.

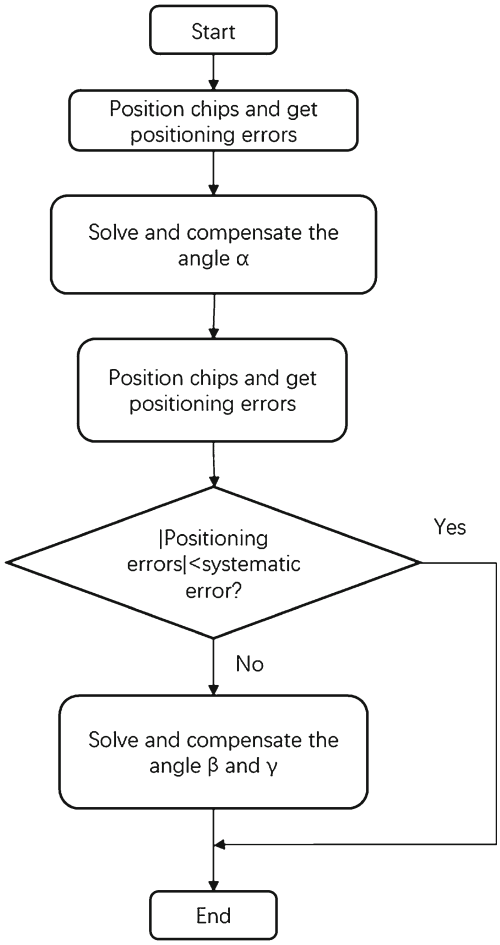

Fig. 15 Calibration algorithm flow diagram

5 Experimental validation

This section is to verify the improved calibration algorithm experimentally from the following perspectives.

5.1 Solving and compensating α

In order to reflect the relationship between the chip positioning errors and the chip position distribution, the "S" positioning order was selected instead of random order, as shown in Fig. 16. After positioning the chips in one image, the positioning errors are shown in Fig. 17. We found that the errors in X direction in the different rows had larger difference relatively and increased gradually from top to bottom in image, while the errors in Y direction in the different columns had also larger difference relatively and decreased gradually from left to right in image, which was consistent with the description in Section 3.3. Selecting five sets of data and solving the angle α with improved calibration algorithm as described in Section 4.2, we obtained $\alpha = 2.78°$. Compensating α and positioning the chips in another image as "S" positioning order, the result showed positioning errors were reduced obviously, as shown in Fig. 18.

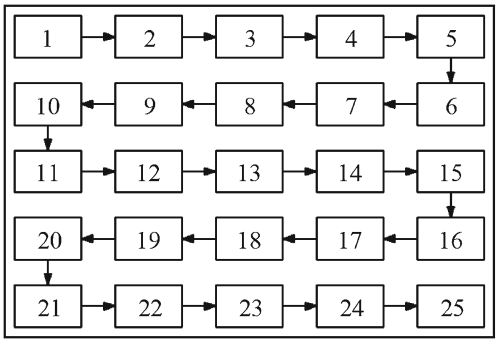

Fig. 16 "S" positioning order in image

5.2 Solving and compensating β and γ

In Section 5.1, after compensating α, the positioning errors was still more than the systematic error ±6 μm, and we considered there were other factors that impact on the poisoning accuracy of the system. As shown in Fig. 18, the errors in X direction in the left side (1, 2, 9, 10, 11, 12, 19, 20, 21, 22) of the image were approximately negative and the errors in the right side (4, 5, 6, 7, 14, 15, 16, 17, 24, 25) were approximately positive, while the errors in Y direction in the bottom side (16, 17, 18, 19, 20, 21, 22, 23, 24, 25) of the image were approximately negative and the errors in the top side (1, 2, 3, 4, 5, 6, 7, 8, 9, 10) were approximately positive, which was also consistent with the description in Section 3.3. Selecting five sets of data and solving the angles β and γ, we obtained $\beta = 0.18°$, $\gamma = 0.60°$. After compensating β and γ and positioning the chips again in another image as "S" positioning order, obviously, the positioning errors were reduced to less than ±6 μm, meeting the accuracy requirement of chip manufacturing, as shown in Fig. 19.

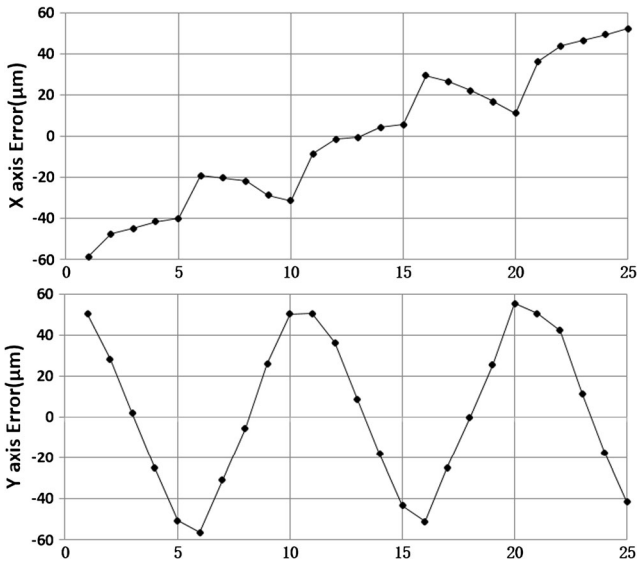

Fig. 17 Before compensating α

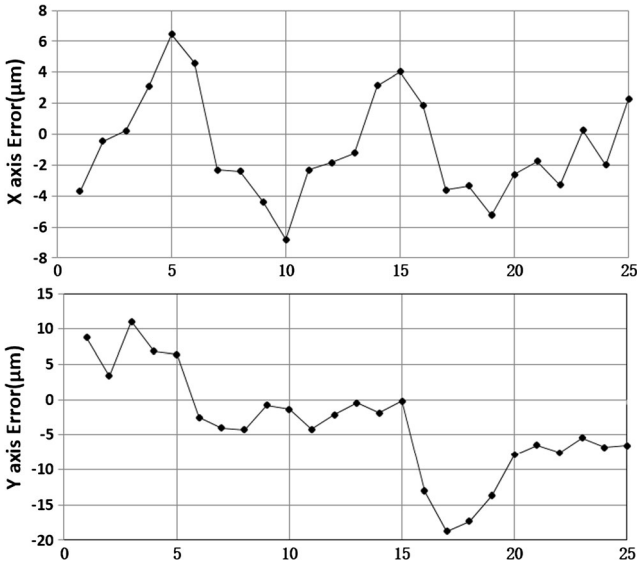

Fig. 18 After compensating α

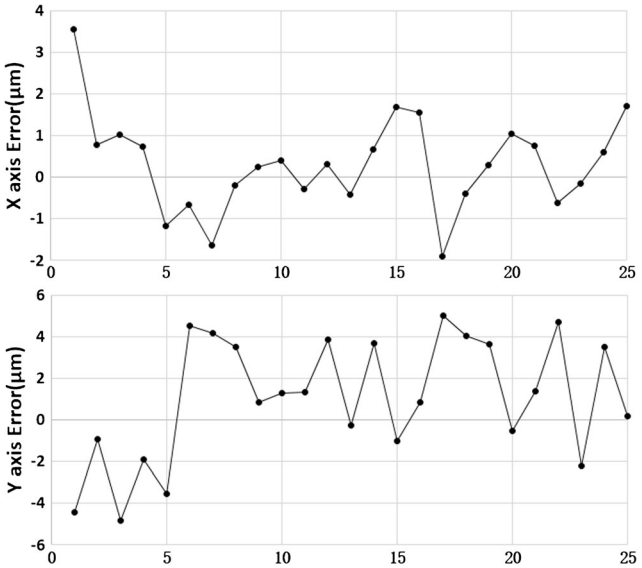

Fig. 20 Test for chips of 35mil

5.3 Robustness and stability test

This section is to verify robustness and stability of the improved calibration algorithm. In order to verify the adaptability to the chips of different types and sizes, we replaced the chips of 25mil with the chips of 35mil, and other conditions remained unchanged. After replacement of wafer, we should adjust the magnification of lens, focal length, and relative location of *X*–*Y* table and vision system to get a clear and satisfactory image. As described in Section 4.1, during the adjusting process, the angles α, β, and γ may vary on a small scale, but inevitably bring unacceptable errors. According to the improved calibration algorithm, solving the calibration parameters α, β, and γ and positioning the chips of 35mil, the experimental result is shown in Fig. 20. We found that the positioning errors after replacement of chips remained less than ±6 μm, and the improved calibration algorithm can adapt to different types and sizes of chips. Generally, the errors caused by calibration algorithm may be magnified with the increase of the distance from the localization point. An image of 25 chips far from the localization point was captured, and these 25 chips were positioned in another test. As shown in Fig. 21, the positioning errors of these chips were also less than 6 μm. In conclusion, the improved calibration algorithm has good robustness and stability, and can satisfy the requirement of high-quality and efficient manufacturing of LED chips.

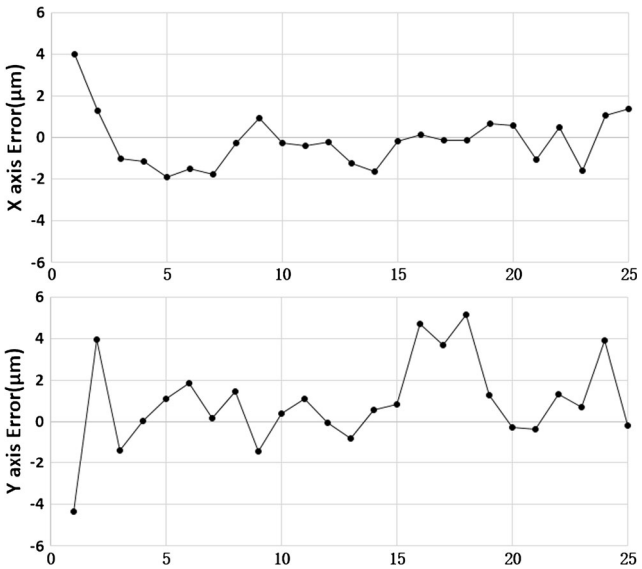

Fig. 19 After compensating β and γ

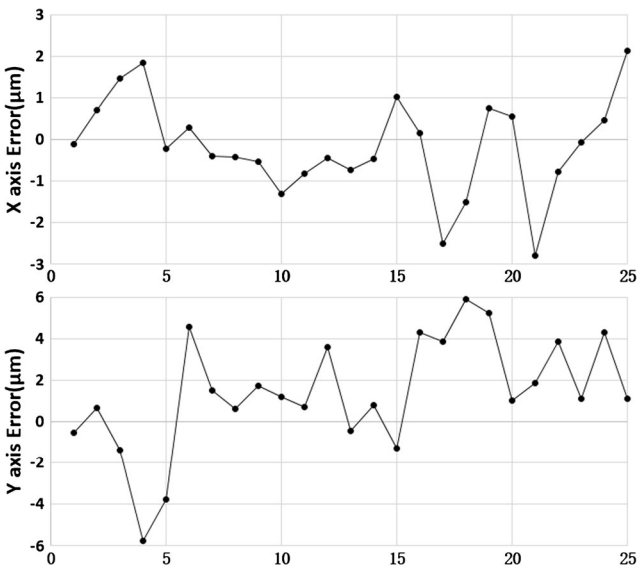

Fig. 21 Test for chips far from the localization point

6 Conclusion

By error analysis of the LED chip localization system based on visual feedback, the relationship of positioning errors of chips and the chip position distribution in image were obtained, and then an improved calibration algorithm was proposed according to the characteristics of chip visual positioning. This algorithm solved calibration parameters (α, β, and γ) in two steps instead of solving transformation matrix at a time with the common calibration algorithm. Considering visual localization system of chips has its own characteristics, we solved α first, and then determine whether β and γ can be solved according to the systematic error. The experimental results indicated that the improved calibration algorithm reduced the positioning errors obviously and had good robustness and stability, meeting the requirement of high efficiency and high precision in LED chip production.

Acknowledgments This work was supported in part by The National Natural Science Foundation of China under Grant No. 51375192 and in part by Science and Technology Support Program of Hubei Province under Grant No. 2014BAA009.

References

1. Wu T, Li B, Wang LW, Huang Y (2010) Automatic detect and match of LED dies basing on position relations between adjacent dies. Proceedings of the Ninth International Conference on Machine Learning and Cybernetics, Qingdao 3:1195–1200. doi:10.1109/ICMLC.2010.5580907
2. Zhong F, He S, Li B (2015) Blob analyzation-based template matching algorithm for LED chip localization. Int J Adv Manuf Technol. doi:10.1007/s00170-015-7638-5
3. Conte J, Majarena AC, Aguado S, Acero R, Santolaria J (2015) Calibration strategies of laser trackers based on network measurements. Int J Adv Manuf Technol 83(5):1161–1170. doi:10.1007/s00170-015-7661-6
4. Faig W (1975) Calibration of close-range photogrammetry systems: mathematical formulation. Photogramm Eng Remote Sens 41(12):1479–1486
5. Abdel-Aziz YI, Karara HM, Hauck M (2015) Direct linear transformation from comparator coordinates into object space coordinates in close-range photogrammetry. Photogramm Eng Remote Sens 81(2):103–107
6. Tsai RY (1986) An efficient and accurate camera calibration technique for 3D machine vision. Proceedings of IEEE Computer Vision and Pattern Recognition Conference 1986:364–374
7. Weng J, Cohen P, Herniou M (1990) Calibration of stereo cameras using a non-linear distortion model [CCD sensory]. International Conference on Pattern Recognition 1:246–253
8. Faugeras OD, Luong QT, Maybank SJ (1992) Camera self-calibration: theory and experiments. European Conference on Computer Vision 588(12):321–334
9. Hartley RI (1994) Projection reconstruction and invariants from multiple images. IEEE Trans Pattern Anal Mach Intell 16(10):1036–1041
10. Triggs B (1997) Autocalibration and the absolute quadric. Conference on Computer Vision and Pattern Recognition 22(8):609–614
11. Bajramovic F, Ckner M, Denzler J (2012) An efficient shortest triangle paths algorithm applied to multi-camera self-calibration. Journal of Mathematical Imaging and Vision 43(2):89–102
12. Pollefeys M, Gool LV, Oosterlinck A (1996) The modulus constraint: a new constraint self-calibration. International Conference on Pattern Recognition 1:349–353
13. Zhao L, Wu C, Liu S (2012) A self-calibration method based on two pairs of orthogonal parallel lines. International Conference on Intelligent Networking and Collaborative Systems 40(9):373–376
14. Galetto M, Mastrogiacomo L, Pralio B (2011) MScMS-II: an innovative IR-based indoor coordinate measuring system for large-scale metrology applications. Int J Adv Manuf Technol 52(1):291–302. doi:10.1007/s00170-010-2717-0
15. Li J, Yang Y, Fu G (2011) Camera self-calibration method based on GA-PSO algorithm. International Conference on Cloud Computing and Intelligence Systems 2011:149–152
16. Akkad NE, Saaidi A, Satori K (2012) Self-calibration based on a circle of the cameras having the varying intrinsic parameters. International Conference on Multimedia Computing and Systems 248(4):161–166
17. Merras M, Akkad NE, Saaidi A, Nazihl AG (2013) A new method of camera self-calibration with varying intrinsic parameters using an improved genetic algorithm. International Conference on Intelligent Systems: Theories and Applications 24(4):1–8. doi:10.1109/SITA.2013.6560799
18. Bellandi P, Docchio F, Sansoni G (2013) Roboscan: a combined 2D and 3D vision system for improved speed and flexibility in pick-and-place operation. Int J Adv Manuf Technol 69(5):1873–1886. doi:10.1007/s00170-013-5138-z
19. Muruganantham C, Jawahar N, Ramamoorthy B, Giridhar D (2008) Optimal settings for vision camera calibration. Int J Adv Manuf Technol 42(7):736–748. doi:10.1007/s00170-008-1634-y
20. Hartley RI (1997) Self-calibration of stationary cameras. Int J Comput Vis 22(1):5–23
21. Ma SD (1996) A self-calibration technique for active vision systems. IEEE Transactions on Robotics & Automation 12(1):114–120
22. Xiong JL, Zhang Q, Xia JY, Peng S (2009) A linear self-calibration method based on active vision system. International Congress on Image and Signal Processing 2009:1–4
23. Shih CL, Ruo CW (2005) Auto-calibration of an SMT machine by machine vision. Int J Adv Manuf Technol 26(3):243–250. doi:10.1007/s00170-003-1765-0
24. Zhan Q, Wang X (2012) Hand–eye calibration and positioning for a robot drilling system. Int J Adv Manuf Technol 61:691–701. doi:10.1007/s00170-011-3741-4